nature genetics



# The Bardet-Biedl protein BBS4 targets cargo to the pericentriolar region and is required for microtubule anchoring and cell cycle progression

Jun Chul Kim[1,6], Jose L Badano[2,6], Sonja Sibold[3,6], Muneer A Esmail[1], Josephine Hill[3], Bethan E Hoskins[3], Carmen C Leitch[2], Kerrie Venner[4], Stephen J Ansley[2], Alison J Ross[3], Michel R Leroux[1], Nicholas Katsanis[2,5] & Philip L Beales[3]

**BBS4 is one of several proteins that cause Bardet-Biedl syndrome (BBS), a multisystemic disorder of genetic and clinical complexity. Here we show that BBS4 localizes to the centriolar satellites of centrosomes and basal bodies of primary cilia, where it functions as an adaptor of the p150$^{glued}$ subunit of the dynein transport machinery to recruit PCM1 (pericentriolar material 1 protein) and its associated cargo to the satellites. Silencing of *BBS4* induces PCM1 mislocalization and concomitant deanchoring of centrosomal microtubules, arrest in cell division and apoptotic cell death. Expression of two truncated forms of BBS4 that are similar to those found in some individuals with BBS had a similar effect on PCM1 and microtubules. Our findings indicate that defective targeting or anchoring of pericentriolar proteins and microtubule disorganization contribute to the BBS phenotype and provide new insights into possible causes of familial obesity, diabetes and retinal degeneration.**

In animal cells, centrosomes have numerous functions, including spindle formation, transport of cytoplasmic organelles, morphogenesis, regulation of cell division and determination of cell shape[1]. The centrosome acts as a microtubule organizing center (MTOC) by nucleating and anchoring microtubules, in a manner similar to that of the spindle pole body in yeast and the blepharoplast in lower plants[1]. Ultrastructural studies have determined that centrosomes consist of a pair of centrioles nearly surrounded by a tube of amorphous material called pericentriolar material[2–4]. Additionally, electron-dense granules called massules or centriolar satellites associate peripherally with centrosomes[5].

Centrioles are thought to organize the pericentriolar material and confer centrosomal stability[6]. They are conserved, microtubule-based structures that localize not only to centrosomes but also to the basal bodies of cilia or flagella. The process by which a mother centriole is converted into a basal body that gives rise to a primary cilium in mammalian cells seems to be cell type–specific and developmentally regulated (reviewed in ref. 7).

In contrast, the composition of centriolar satellites is poorly defined. One component is PCM1, a 228-kDa autoantigen recognized by anti-centrosome serum[4,8]. PCM1 has a dynamic cellular distribution, localizing with centrosomal satellites throughout the cell cycle except during metaphase and anaphase, when it becomes cytosolic[8,9]. PCM1 acts as a scaffold for several proteins, including centrin, pericentrin, kendrin/pericentrin B and ninein, and is transported to the centrosome in a microtubule-dependent manner by the dynein-dynactin molecular motor[2].

The cellular localization of PCM1 indicates that the material surrounding centrosomes and the material surrounding basal bodies are molecularly related. PCM1 is thought to be involved in recruiting proteins necessary for centrosome replication and in organizing or anchoring microtubules emanating from the MTOC[2,9]. PCM1 is also a component of fibrous granules, electron dense particles that form during ciliogenesis and basal body replication, which suggests that fibrous granules and centriolar satellites may be equivalent nonmembranous organelles[4]. Together, these observations suggest that PCM1 participates in the biogenesis, function and maintenance of both centrosomes and cilia[2,4].

BBS (OMIM 209900) is a heterogeneous disorder characterized by retinal dystrophy, renal dysfunction, obesity, polydactyly and numerous developmental and behavioral defects[10]. It is typically inherited in an autosomal recessive fashion, although in some families three mutations in two genes are required for pathogenesis[11]. Six of at least eight genes associated with BBS have been cloned; they encode proteins of

[1]Department of Molecular Biology and Biochemistry, Simon Fraser University, 8888 University Dr., Burnaby BC, V5A 1S6, Canada. [2]Institute of Genetic Medicine, Johns Hopkins University, 600 North Wolfe Street, Baltimore, Maryland 21287, USA. [3]Molecular Medicine Unit, Institute of Child Health, University College London, London WC1N 1EH, UK. [4]Department of Electron Microscopy, Institute of Neurology, Queens Square, London, UK. [5]Wilmer Eye Institute, Johns Hopkins University, 600 North Wolfe Street, Baltimore, Maryland 21287, USA. [6]These authors contributed equally to this work. Correspondence should be addressed to M.R.L. (leroux@sfu.ca) or N.K. (katsanis@jhmi.edu).

Published online 25 April 2004; doi:10.1038/ng1352

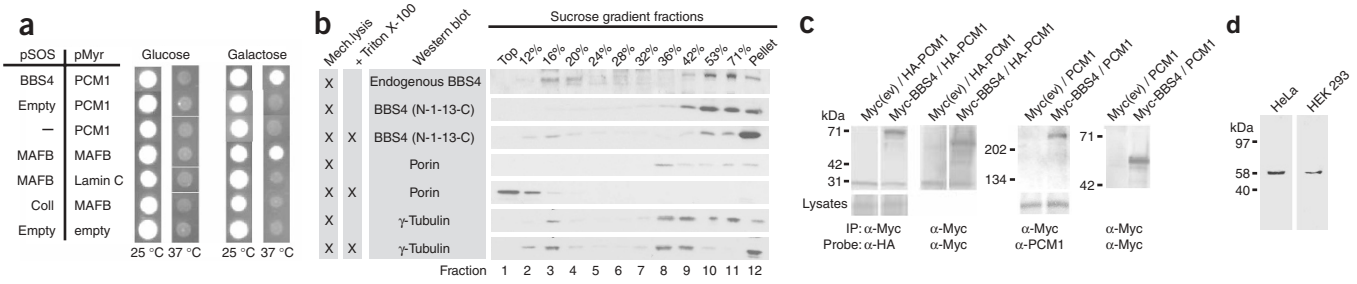


**Figure 1** BBS4 interacts with PCM1. (**a**) BBS4 interacts with PCM1 in yeast two-hybrid analysis. Positive (MAFB, which homodimerizes) and negative (MAFB and Lamin C, Coll and MAFB) controls are shown. (**b**) Discontinuous sucrose gradient analysis. BBS4 is present in high-molecular-weight fractions coinciding with centrosomal γ-tubulin (fractions 10 and 11). Porin is a mitochondrial protein released to a soluble form in detergent. (**c**) Left panels, 2.2 mg of protein from cell lysates of HEK 293 cells transiently expressing constructs (as indicated) were immunoprecipitated with antibody to Myc and western-blotted with antibody to HA. Myc-BBS4 but not Myc–empty vector (ev) coimmunoprecipitated with PCM1 (HA-PCM1, ~70-kDa species). Right panels, Myc-BBS4 interacts with endogenous PCM1. 10 mg of protein from lysates of cells transfected with Myc-BBS4 were immunoprecipitated with antibody to Myc and western-blotted with antibody to PCM1. The control Myc-BBS4 expression is also shown. (**d**) Western blot of total HeLa and HEK 293 protein extracts with affinity-purified polyclonal antibody to BBS4.

unknown function: BBS1, BBS2, BBS4, BBS6, BBS7 and BBS8 (refs. 12–18). The resemblance of various BBS phenotypes to disorders caused by improper cilia function suggests that BBS might be of the same etiology[18,19]. Notably, the recent identification and expression studies of mammalian and *C. elegans BBS* orthologs suggest that BBS may be caused by defects in centrosomes, basal bodies and cilia, or both[18], but the functions of BBS proteins are not yet known.

Here we report the first direct evidence for the cellular mechanism of BBS pathogenesis. We show that BBS4 localizes to the centriolar satellites of centrosomes and basal bodies and is necessary to recruit PCM1 to centrosomal satellites, probably by acting as an adaptor between PCM1 and the dynein-dynactin motor complex. Ablation of BBS4 results in PCM1 mislocalization, loss of microtubule anchoring at the centrosome, defects in cytokinesis and apoptosis. Our data model both the null mutations and truncating mutations in *BBS4* observed in some individuals with BBS. Therefore, we suggest that at least some of the molecular defects of BBS are caused by improper targeting of PCM1 and its associated proteins to centriolar satellites and by severe microtubule disorganization that disrupts the proper function of both centrosomes and basal bodies.

## RESULTS

### Domain composition of BBS4

Sequence analysis of human and mouse BBS4 proteins have not identified significant similarity to any proteins of known function. To investigate the domain structure of BBS4, we carried out homology searches and scanned the SMART protein domain database[20]. We detected as many as 13 tandem tetratricopeptide repeat (TPR) motifs flanked by short N- and C-terminal regions (**Supplementary Fig. 1** online). TPRs are composed of degenerate stretches of 34 amino acids that fold into

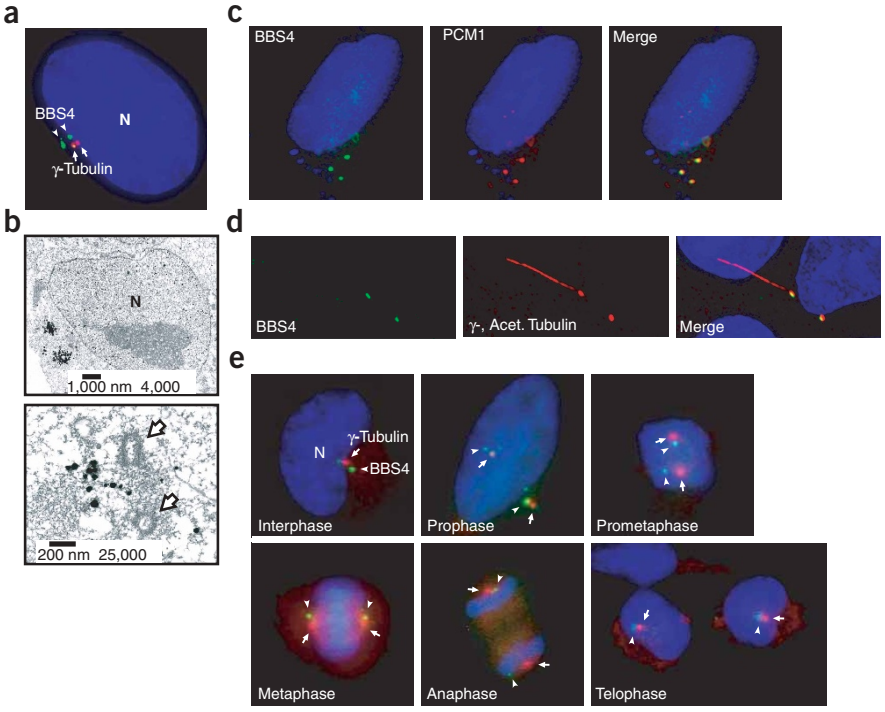


**Figure 2** BBS4 is a pericentriolar protein associated with centrosomes and basal bodies. (**a**) Coimmunofluorescence staining in HeLa cells using antibodies against endogenous BBS4 (green) and γ-tubulin (red). (**b**) Transmission electron micrographs of immunogold-stained BBS4 shows perinuclear (top panel) and pericentriolar (bottom panel) electron-dense spots. Arrows indicate centrioles; N represents the nucleus. (**c**) Deconvolution images showing that BBS4 (green, left panel) and PCM1 (red, middle panel) overlap in HeLa cells (yellow, right panel). (**d**) BBS4 (green, left panel) localizes near the mother centriole (basal body emanating a primary cilium) and daughter centriole (middle and right panels) in IMCD3 cells. Centrioles are detected with antibody to γ-tubulin; the cilium is stained with antibody to acetylated tubulin (both red). (**e**) BBS4 remains pericentrosomal during the cell cycle. Synchronized HeLa cells were costained with antibodies against BBS4 and γ-tubulin. Arrowheads indicate BBS4 signals (green), and arrows indicate γ-tubulin staining (red). Cell cycle stages are indicated in each panel.

characteristic helix-turn-helix structures and typically occur as single or multiple triplet arrays. These usually mediate protein-protein interactions by cradling a specific linear peptide sequence[21].

### BBS4 interacts with the C terminus of PCM1

Our domain analyses suggested that BBS4 might function in a multisubunit complex and that identifying other members of this complex might clarify its function. We therefore carried out a yeast two-hybrid screen with full-length *BBS4* cDNA as bait and a fetal brain cDNA library as prey. We then selected five clones that fulfilled our selection criteria. Two clones contained different but overlapping fragments of PCM1, a pericentriolar protein that recruits several centrosomal components[9]. One of these encoded a C-terminal portion of PCM1 (residues 1,574–2,024), and the other encoded a smaller region (residues 1,744–2,024). We confirmed the specificity of the yeast two-hybrid interaction in several control experiments (**Fig. 1a**). A second yeast two-hybrid screen of a human kidney cDNA library with *BBS4* as bait also identified independent clones containing coding regions of PCM1 (1,845–2,024 and 1,913–2,024, respectively; data not shown). These data suggested that BBS4 can bind to the C-terminal 112 amino acids of PCM1.

To corroborate the BBS4-PCM1 interaction by coimmunoprecipitations in mammalian cells, we first determined the biochemical behavior of BBS4 using discontinuous sucrose gradient fractionation. Endogenous and Myc-tagged BBS4 sedimented in a similar manner at a high-molecular-weight position (fractions 10 and 11; **Fig. 1b**). Most endogenous and Myc-tagged BBS4 from mechanically lysed cell extracts sedimented to a position similar to that of centrosomal γ-tubulin (fractions 10 and 11), an established centrosomal marker. Lysis by Triton X-100 caused most of the BBS4 and of the detergent-insoluble centrosomal γ-tubulin to pellet. Some γ-tubulin is not centrosomal and complexes with the chaperonin CCT[22] (fraction 3) or with other soluble cellular components[23] (fractions 8 and 9). Because some Myc-BBS4 (**Fig. 1b**, Fraction 3) and hemagglutinin (HA) epitope-tagged PCM1 (**Fig. 1c**) is solubilized in the presence of detergent, we used the supernatant of this extract as the starting material for immunoprecipitations.

Transfection of epitope-tagged vectors into HEK 293 cells followed by immunoprecipitation showed that the HA-PCM1 fragment coprecipitated with Myc-BBS4 (**Fig. 1c**). The immunoprecipitation was specific, as the HA-PCM1 fragment was not recovered by immunoprecipitating extracts of cells coexpressing pCMV-HA-PCM1 and an empty pCMV-Myc vector (**Fig. 1c**). The two proteins also coimmunoprecipitated with the tags reversed (data not shown). More importantly, we also observed seminative interaction between Myc-BBS4 and endogenous PCM1 using a polyclonal antibody to PCM1 (**Fig. 1c**).

### BBS4 is a pericentriolar protein colocalizing with PCM1

We next generated a polyclonal antibody against BBS4 to probe whether it colocalized with PCM1. In a western blot with extracts from HeLa or HEK 293 cells, the antibody to BBS4 cross-reacted with a single protein species of the expected molecular weight (**Fig. 1d**). Using this antibody, we found that endogenous BBS4 localized to the pericentriolar region of various mammalian cells, including HeLa, HEK 293, NIH 3T3, IMCD3 and COS-7 cells (**Fig. 2a** and data not shown). Consistent with the sucrose gradient data, the localization of epitope-tagged BBS4 was identical to that of the endogenous protein (**Fig. 3c**). We refined these data by determining the ultrastructural localization of BBS4. In silver-enhanced, resin-embedded cells visualized by transmission electron microscopy, we confirmed that BBS4 localized as distinct aggregates adjacent to, but not directly associated with, the two centrosomal centrioles. The aggregates were not membrane-bound and were often found as pairs, typically spaced 0.5–1 m apart (**Fig. 2b**). We also observed signal overlap for endogenous PCM1 and BBS4 in several cell types (such as HeLa and HEK 293; **Fig. 2c**). Together, these data indicate that BBS4 is a component of centriolar satellites.

Given that one of a pair of centrosomal centrioles (mother centriole) is recruited to the cell apex to serve as a basal body in ciliated cells, we investigated whether BBS4 also colocalized to the basal body of primary cilia, like PCM1 (refs. 4,9). In ciliated IMCD3 cells, costaining with γ- and acetylated tubulin showed that BBS4 was specifically associated with both the basal body and the daughter centriole (**Fig. 2d**).

We next examined whether BBS4 had cell-cycle-dependent differences in behavior. In contrast to PCM1, endogenous BBS4 was associated with the centrosome throughout the cell cycle (**Fig. 2e**), even during metaphase and anaphase when PCM1 disperses[8,9]. This suggested that BBS4 localizes to the pericentriolar region in a PCM1-independent manner.

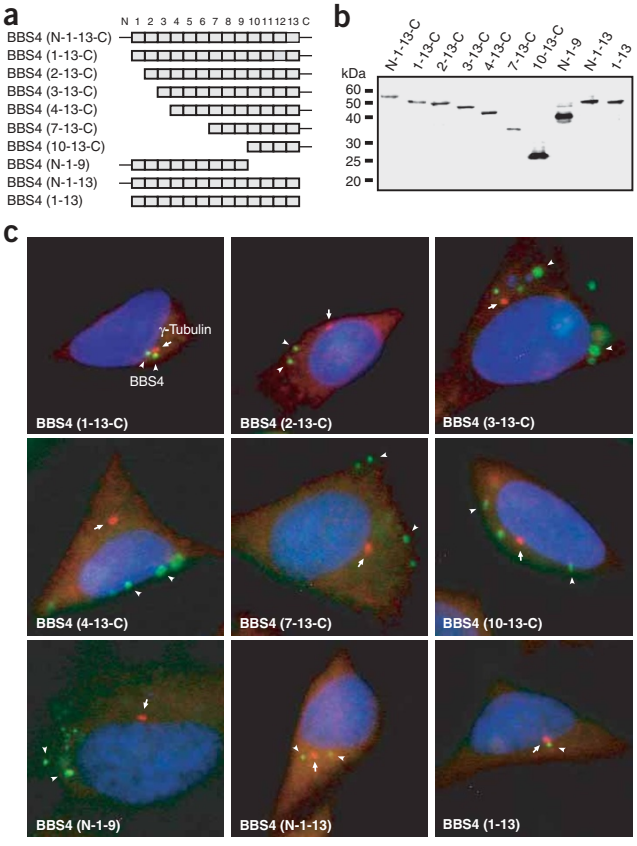


**Figure 3** Localization of BBS4 to centrosomal satellites depends on both N- and C-terminal TPRs. (**a**) Schematic representation of Myc-tagged full-length BBS4 and of nine truncation mutants. The nomenclature of the constructs and the sequences of the different BBS4 segments is detailed in **Supplementary Figure 1** online. (**b**) Western blot (using an antibody to Myc) of extracts from HeLa cells expressing Myc-tagged full-length and truncated BBS4 constructs shows that the proteins produced are of the predicted size. (**c**) Immunolocalization of the Myc-tagged truncated BBS4 constructs in HeLa cells. BBS4 was detected using an antibody to Myc, and cells were costained with γ-tubulin. Arrowheads indicate BBS4 signals (green), and arrows indicate γ-tubulin signals (red).

### BBS4 mutants exert a dominant-negative effect on PCM1

To investigate further the function of BBS4 and explore its relationship with PCM1, we determined which regions of BBS4 were required for localization to centriolar satellites and for binding to PCM1. We constructed and expressed in HeLa cells a panel of nine Myc-tagged BBS4 deletion mutants lacking one or both of the terminal regions and up to 9 of the 13 predicted TPR motifs (**Fig. 3a**,**b**). Immunofluorescence analysis with an antibody to Myc showed that deletion of either or both BBS4 terminal regions had no effect on its pericentriolar localization (**Fig. 3c**). In contrast, BBS4 variants lacking the N-terminal region and the first predicted TPR (construct 2-13-C) and additional TPRs (constructs 3-13-C, 4-13-C, 7-13-C and 10-13-C) consistently failed to localize near the centrosome. Similarly, the BBS4 deletion mutant N-1-9 was also scattered in the cytoplasm as punctate spots (**Fig. 3c**).

We then probed whether the BBS4 truncation mutants could interact effectively with PCM1. Using HeLa cells transiently expressing the Myc-BBS4 deletion mutants, we tested for an overlap in immunofluorescence signal with endogenous PCM1. BBS4 mutants containing the third predicted TPR motif (2-13-C, 3-13-C and N-1-9) mislocalized with endogenous PCM1 (**Fig. 4a**) as cytoplasmic granules. Because endogenous BBS4 was present in these cells, the truncated forms of the protein probably acted in a dominant-negative manner to prevent proper PCM1 localization. Consistent with this observation, immunoprecipitations indicated that only the BBS4 deletion mutants that mislocalized with PCM1 (constructs 2-13-C, 3-13-C and N-1-9) retained an appreciable ability to interact with PCM1 (**Fig. 4b**). In contrast, other mislocalized BBS4 mutants that interacted weakly or not at all with PCM1 (constructs 4-13-C, 7-13-C and 10-13-C; **Fig. 4b**) had no appreciable effect on the localization of PCM1 near the centrosome (**Fig. 4a**), probably because it could interact with endogenous BBS4.

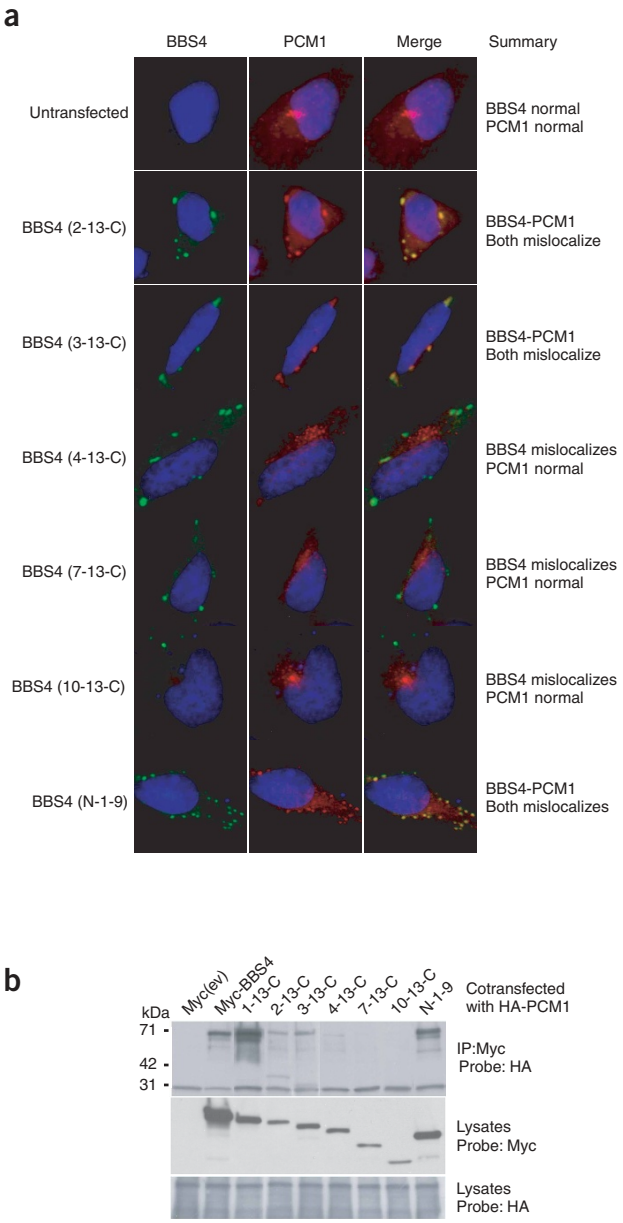


### Dynein is necessary for proper BBS4 localization

Previous studies reported that PCM1 depends on dynein-dynactin for its retrograde transport along microtubules[8,9], whereas other centrosomal proteins, such as γ-tubulin, do not[2]. We therefore examined whether BBS4 was targeted to centriolar satellites in a dynein-dependent manner by determining its cellular location in cells overexpressing p50-dynamitin, which antagonizes dynactin function[24]. First, we confirmed that HeLa cells overexpressing Myc-tagged p50-dynamitin had mislocalized PCM1 but not γ-tubulin (**Fig. 5a**). We then observed that, as with PCM1, cells transfected with p50-dynamitin showed loss of the BBS4 perinuclear signal (**Fig. 5a**).

In parallel, yeast two-hybrid screening identified the $p150^{glued}$ subunit of dynactin as an interacting partner of BBS4 (**Fig. 5b**). We substantiated this finding by observing that BBS4 and $p150^{glued}$ expressed in HEK 293 cells coimmunoprecipitated specifically (**Fig. 5c**). Sequence analysis of yeast constructs expressing partial $p150^{glued}$ protein fragments indicated that the C terminus of $p150^{glued}$ (amino acids 1,022–1,170) was sufficient to mediate interaction with BBS4. $p150^{glued}$ physically links dynein to dynactin and is a key factor in modulating the function and cargo binding of the dynein molecular motor[25]. As the region of interaction with BBS4 lies outside those regions of $p150^{glued}$ required for binding microtubules (amino acids 39–150; ref. 26) and dynein intermediate chain (amino acids 200–811; ref. 24), this interaction suggests that BBS4 is transported to the pericentriolar region by the dynein-dynactin complex.

### Loss of BBS4 function results in PCM1 dispersal

To probe the function of BBS4 further, we depleted BBS4 from mammalian cells by using RNA interference (RNAi). To ensure maximum specificity of targeting, we adopted several independent approaches.

**Figure 4** Incorrect localization of BBS4 affects the behavior of PCM1. (**a**) Localization of PCM1 to the pericentrosomal region is abrogated when certain Myc-tagged truncated BBS4 constructs are expressed in HeLa cells. Costaining with antibodies against Myc (left panels, green) and endogenous PCM1 (middle panels, red) shows proper PCM1 localization in untransfected cells and cells expressing BBS4 (4-13-C, 7-13-C, 10-13-C) and mislocalization with BBS4 in cells expressing BBS4 (2-13-C, 3-13-C and N-1-9). (**b**) Interaction of truncated BBS4 proteins with PCM1 is assessed by coimmunoprecipitations. HEK 293 cells were transfected with each Myc-tagged truncated BBS4 construct. Equal amounts (~2.5 mg) of protein extracts were immunoprecipitated with an antibody to Myc and western-blotted with antibody to HA to detect HA-PCM1 (~70 kDa). Deletion of the third TPR domain in BBS4 substantially weakened the BBS4-PCM1 interaction (compare 3-13-C with 4-13-C), whereas deletion of additional TPRs abolished all detectable interaction. ev, empty vector.

Transfection of HeLa cells with BBS4 small interfering RNA (siRNA) sequences resulted in loss of *BBS4* on a northern blot at both 48 h and 72 h after transfection (**Fig. 6a**). Real-time RT-PCR also indicated that *BBS4* mRNA was 30 times less abundant (data not shown). The successful knockdown of BBS4 was further confirmed by immunocytochemistry with an antibody to BBS4 (**Fig. 6b**). By observing >100 cells in multiple independent experiments, we estimated that most cells transfected with pSUPER-BBS4 or pSilencer-BBS4 (≥90%) gave no perceptible immunofluorescence signal compared with control cells (**Fig. 6b**). The targeting was specific to *BBS4*, as scrambling the oligo sequence gave no loss of *BBS4* and targeting other genes by RNAi, including *BBS2*, did not affect *BBS4* expression as judged by real-time RT-PCR (data not shown). We transfected pSUPER-BBS4 into HeLa cells and assessed the cellular phenotype. We observed that in the absence of BBS4, PCM1 became completely dispersed in the cytosol (**Fig. 6c**). We confirmed this effect, and found it to be specific, by analyzing COS-7 cells transfected with three different pSilencer-BBS4 vectors (encoding different siRNA sequences) and by observing HeLa and HEK 293 cells transfected with three different synthesized siRNA sequences (data not shown).

We also addressed whether the organization of the microtubule network was disrupted in BBS4 knockdown cells. In addition to HeLa or HEK 293 cells, we examined COS-7 cells because they have a distinct, MTOC-radiating microtubule array (**Fig. 6d**). When transformed with three different pSilencer-BBS4 knockdown vectors, but not with a control vector, COS-7 cells had a conspicuous microtubule staining pattern consistent with a failure to anchor at the centrosome; in all cells showing loss of BBS4 signal, and therefore PCM1 mislocalization, the microtubule network either showed a disorganized array emanating crudely from the outer edges of the nucleus or was extensively dispersed and formed bundles near the cell periphery (**Fig. 6d**). This phenotype was due to defective microtubule anchoring, not nucleation, as regrowth of microtubules in control cells and BBS4-depleted cells was essentially identical after transient treatment with nocodazole (**Fig. 6e**).

HeLa cells depleted of BBS4 fail to divide. This implicates BBS4 in cell cycle processes. Furthermore, individual BBS4-depleted cells often had two or more nuclei of variable sizes (**Fig. 6f**). Notably, such multinucleated cells always contained replicated centrioles, as we consistently observed more than two distinct γ-tubulin spots (**Supplementary Fig. 2** online). To investigate this phenotype further, we carried out fluorescence-activated cell sorting (FACS) cell cycle analyses on COS-7 control cells, cells treated with nocodazole and mimosine and cells transfected with two different pSilencer-BBS4 vectors (**Fig. 6g** and **Supplementary Fig. 2** online). Control cells had a normal cell cycle profile with most cells in the G1 phase (2n DNA content) and smaller cell populations undergoing DNA replication (S phase) and in the G2/M phase (4n DNA content); treatment with nocodazole, as expected, arrested cells in the G2 phase. A small proportion of nocodazole-treated cells were also apoptotic (<2n DNA content) or had a DNA content >4n—an indication of two rounds of DNA replication without cytokinesis. BBS4 knockdown cells had substantially fewer cells in G1 phase and concomitantly more apoptotic cells and cells with a DNA content >4n, suggesting that a proportion of BBS4-depleted cells failed to undergo cell division. Indeed, cell counting experiments showed that BBS4-depleted HeLa cells had few or no cell duplications compared with control cells (data not shown).

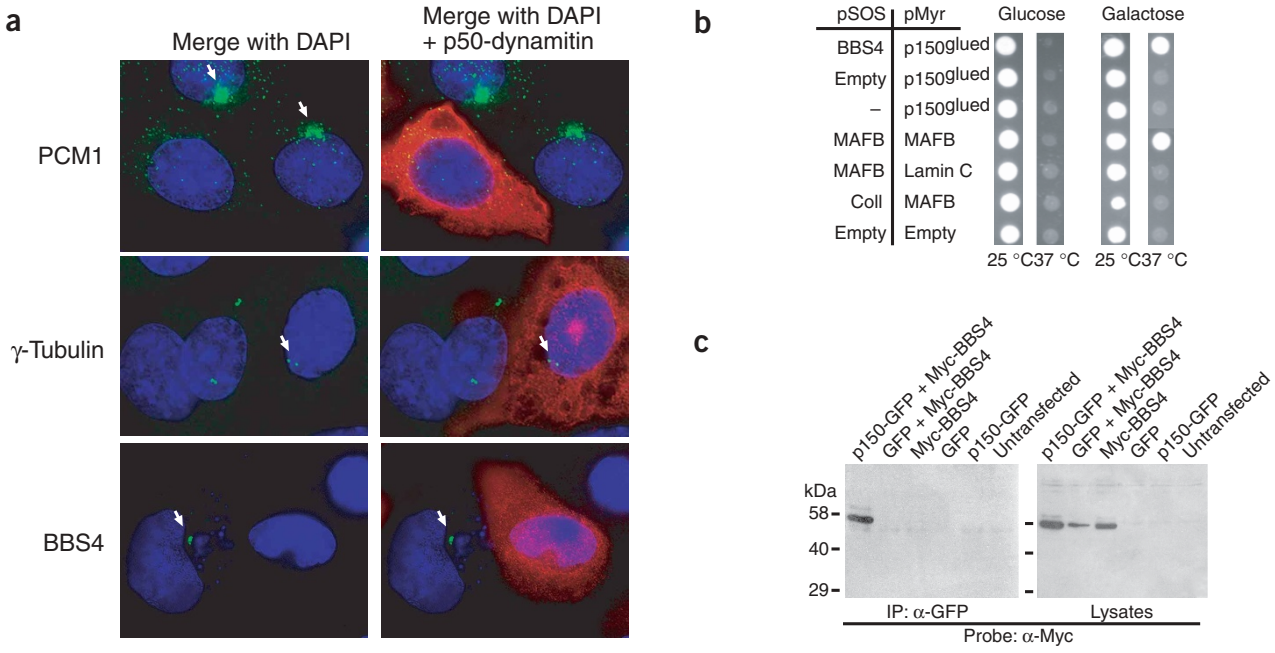


**Figure 5** BBS4 dependence on, and interaction with, the dynein complex. (**a**) HeLa cells were transfected with Myc-tagged p50-dynamitin to inhibit dynein function and were costained with different antibodies. Top panels, correct PCM1 localization (green) in untransfected cells (left panel) but diffuse cytosolic staining in cells transfected with p50-dynamitin (red, right panel). Middle panels, localization of γ-tubulin (red, shown with an arrow in the left panel) is not affected by p50-dynamitin overexpression (green, right panel). Bottom panels, the correct location of BBS4 in untransfected cells (arrowhead, left panel) and the loss of perinuclear signal in cells transfected with p50-dynamitin (right panel). (**b**) BBS4 interacts with $p150^{glued}$ in yeast two-hybrid analysis. Positive and negative controls are shown. (**c**) Western blotting of cell extracts expressing $p150^{glued}$-GFP, Myc-BBS4 or empty vectors show specific interaction between BBS4 and $p150^{glued}$, as immunoprecipitated Myc-BBS4 can be detected only in the presence of GFP-$p150^{glued}$.

We confirmed that BBS4-depleted cells were prone to undergo apoptosis by using the terminal deoxynucleotidyl transferase–mediated dUTP nick end-labeling (TUNEL) assay. siRNA-treated cells had a substantially greater proportion of apoptotic cells (12.5% and 7.6% for Si27 and Si831 siRNAs, respectively) compared with untreated cells (0.4%) or with cells transfected with a scrambled siRNA sequence (0.2%; **Fig. 6h**).

### BBS4 and PCM1 localize to tissues relevant to BBS

The severe effect of disrupting the function of BBS4 in cultured mammalian cells might suggest that null mutations are not compatible with viability in humans, but this is not the case. But the BBS4-PCM1 interaction may be found in only a subset of differentiated cell types whose malfunction would not compromise organismal viability but may account for the specific, yet pleiotropic, BBS phenotype. To investigate this, we determined the relative localization of BBS4 and PCM1 by staining consecutive sections of various mouse organs and embryos with antibodies to BBS4 and PCM1. Each protein was expressed in only a subset of tissues, and BBS4 and PCM1 colocalized in some, but not all, cell types. For example, we detected identical staining in the cell bodies of neurons in the adult hippocampus and dentate gyrus (**Fig. 7a**,**b**). Consistent with the predicted involvement of both proteins with ciliogenesis and ciliary function[4,18], we observed identical localization in several ciliated tissues, including the ciliated border of bronchioles (**Fig. 7c**,**d**) and olfactory epithelium (**Fig. 7i**,**j**). In the retina, BBS4 was expressed in several layers, but the two proteins colocalized only in the inner photoreceptor segment and not in the outer nuclear layer (**Fig. 7e**,**f**). Such specific colocalization was also found in other tissues, such as the developing pericardium and interdigital epithelium, but not in chondrocytes (**Fig. 7g**,**h**,**k**,**l**).



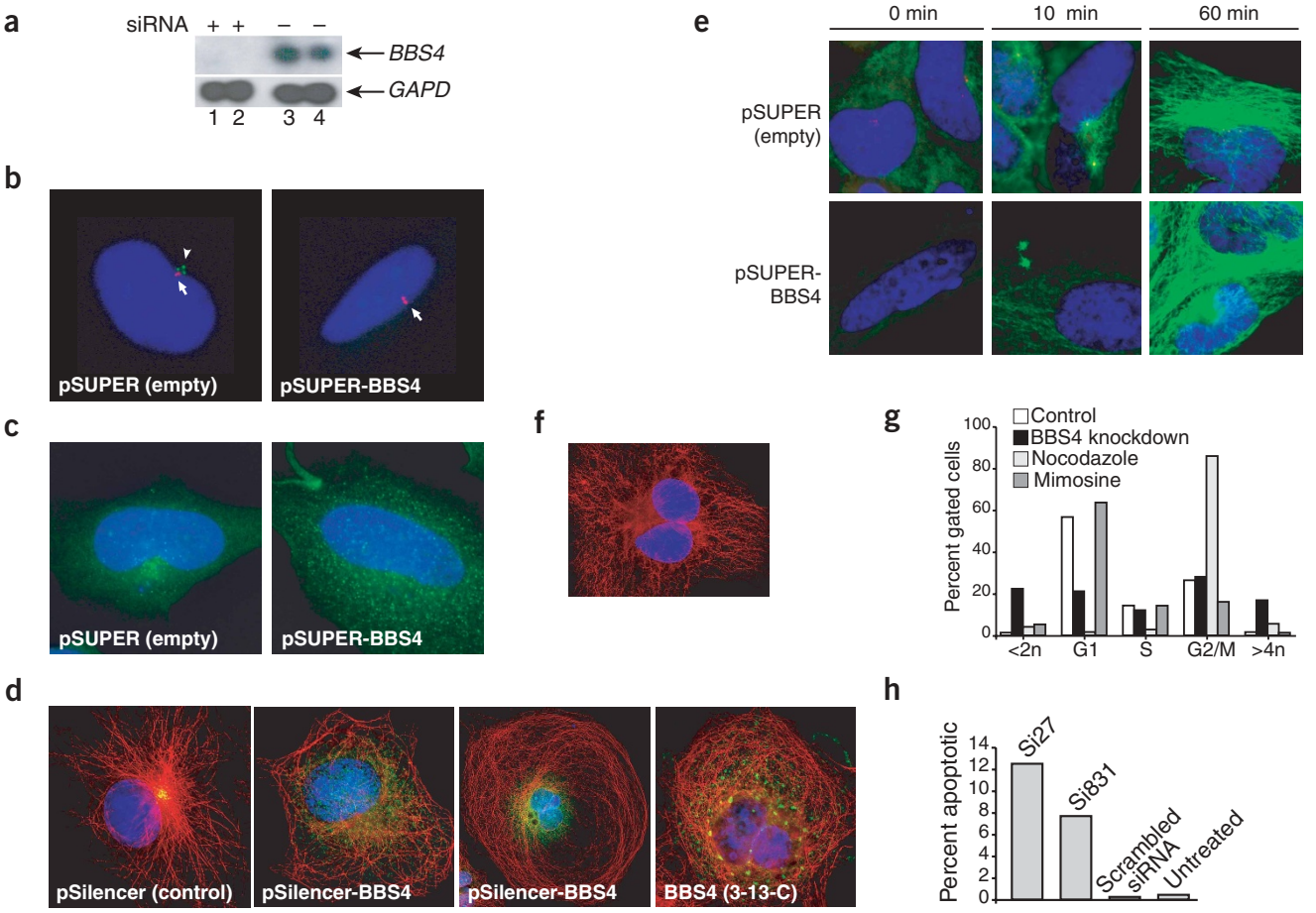


**Figure 6** Loss of BBS4 function. (**a**) Northern blot of HeLa cells untransfected and transfected with siRNA oligos at 24 h (lanes 1 and 3) and 72 h (lanes 2 and 4) after transfection. (**b**) Endogenous BBS4 (green, arrowhead) is detected near the centrosome (detected by γ-tubulin in red; arrow) in cells transfected with empty vector (left panel) but not in cells transfected with pSUPER-BBS4 (right panel). (**c**) HeLa cells transfected with pSUPER-BBS4 (right panel) but not with empty vector (left panel) show dispersed PCM1 signal. (**d**) Compared with empty vector, COS-7 cells expressing pSilencer-BBS4 knockdown vector (two middle panels, PCM1 staining in green) or Myc-tagged BBS4 (3-13-C; green, right panel) have disorganized tubulin staining patterns (with antibody to α-tubulin; red). Cells are costained with antibodies to PCM1 (left and middle panels) and to Myc (right panel). (**e**) Microtubule nucleation and regrowth after nocodazole treatment is as efficient in BBS4-depleted HeLa cells (lower panels) as in untransfected cells (upper panels). Microtubules were immunostained with antibody to α-tubulin at the time points shown. (**f**) Binucleated COS-7 cell expressing pSilencer-BBS4 construct. (**g**) Graph showing the results from FACS analyses of COS-7 control cells (white bars), cells expressing pSilencer-BBS4 (black) and cells treated with nocodazole (light gray) or mimosine (dark gray). The *y* axis shows the percentage of cells with DNA staining intensities corresponding to <2n, G1, S and G2/M and >4n, as shown on the *x* axis. (**h**) Graph of the results from TUNEL assays of untreated HeLa cells or cells transfected with siRNA oligonucleotides (Si27 and Si831) or a scrambled siRNA sequence. The *y* axis shows the percentage of apoptotic cells in each category.

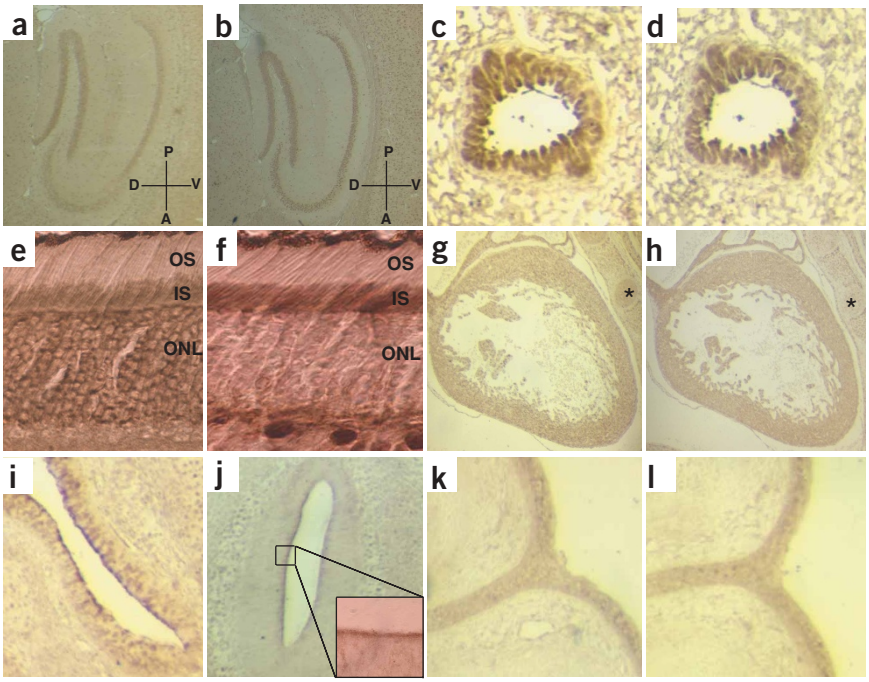


**Figure 7** Histological localization of BBS4 and PCM1. BBS4 (**a**) and PCM1 (**b**) have identical localization throughout the adult mouse hippocampus and dentate gyrus. The cross indicates dorsoventral (DV) and anteroposterior (AP) orientation. (**c**,**d**) In the adult mouse lung, both proteins are found in columnar epithelial cells of bronchioles. (**e**) Adult mouse retina showing BBS4 in the outer nuclear layer (ONL) and the inner segment (IS). By contrast, PCM1 is detected in the inner segment but not the outer nuclear layer (**f**). OS, outer segment. (**g**,**h**) BBS4 and PCM1 are both detectable in the pericardium of an E16 mouse embryo, but only BBS4 can be detected in chondrocytes (asterisk). (**i**,**j**) Both proteins are prominent in the olfactory epithelium. Inset, a magnified image of the boxed area, with most of the signal concentrated at the ciliated border. (**k**,**l**) Strong expression of BBS4 and PCM1 in the epidermal layer surrounding the digits of an E16 mouse embryo. All images are at 10 magnification, except **e**, **f** and the inset in **j**, which are at 64 magnification.



## DISCUSSION

In this study, we found that BBS4 is a pericentriolar protein with a central role in recruiting cargo to centriolar satellites and allowing for the formation of a functional centrosomal MTOC. From our data, we propose a model in which BBS4 forms a stable complex with PCM1 and both proteins colocalize to the centriolar satellites of centrosomes (**Fig. 8**). Loss of BBS4 results in dispersal of PCM1 to the cytosol, loss of microtubule radiation from the centrosome, alteration of cell cycle dynamics and a higher incidence of apoptotic cell death. Given that PCM1 is necessary for recruiting several proteins to the centrosome and required for microtubule anchoring and cell cycle progression[4,9,27,28], we propose that at least some of the cellular defects in BBS4-deficient cells are due to a loss of a functional interaction between BBS4 and PCM1.

BBS4 also interacts with the p150$^{glued}$ subunit of the dynactin-dynein microtubule-based molecular motor, suggesting that BBS4 is directly involved in the transport of PCM1 to the centrosomal satellites by acting as a dynein-associated adaptor protein. Evidence for this hypothesis comes from our observation that disrupting dynein function prevented BBS4 and PCM1 from coalescing near the centrosome. Alternatively, or in addition, both proteins may be trafficked independently and the specific interaction of BBS4 with PCM1 may be needed only to retain PCM1 in its correct cellular location.

The discrete spatial correlation of BBS4 and PCM1 in embryonic and adult tissues might also elucidate the cellular pathogenesis of the disease. For instance, some cognitive aspects of the BBS phenotype might result in part from dysfunction of the hippocampus or the dentate gyrus, where both BBS4 and PCM1 are highly expressed in the cell bodies of neurons but not in axons. Likewise, in the retina, dysfunction at the inner segment (and possibly the connecting cilium) might lead to photoreceptor degeneration. Such hypotheses will require *in vivo* models for validation. Nonetheless, examination of cell types in which BBS4 and PCM1 colocalize could provide insight into the pathogenesis of BBS, as such cells are likely to be either absent or compromised as a consequence of loss-of-function mutations in *BBS4*.

BBS is a multisystemic disorder of particular interest owing to its clinical overlap with complex traits that are prevalent in the general population, including obesity, asthma and diabetes. To our knowledge, BBS is the first pleiotropic phenotype attributed to pericentriolar dysfunction, providing the opportunity to investigate the role of BBS4 and other pericentriolar proteins in complex traits that are key health problems and are poorly understood.

## METHODS

**Yeast two-hybrid screen.** We carried out the cytotrap and Gal-4 yeast two-hybrid screens as described[18]. We amplified the complete open reading frame of *BBS4* from cDNA by PCR using forward and reverse primers tagged with *Sal*I and *Not*I and cloned it into the pSOS vector (bait; Stratagene) or pGBDU. We used a fetal brain library (Stratagene) for the cytotrap and a kidney library (Clontech) in the Gal-4 screen.

**DNA constructs.** We generated cDNAs encoding full-length or truncated BBS4 proteins by PCR using different sets of 5′ and 3′ primers containing *Sal*I and *Not*I restriction sites, respectively, and subcloned them into the expression vector pCMV-Myc (Clontech). BBS4 deletion constructs encode the amino acids corresponding to those detailed in **Supplementary Figure 1** online. The Myc-tagged p50-dynamitin expression vector was a gift from R. Vallee (Columbia University).

**Antibodies.** We generated polyclonal antibodies by immunizing rabbits with two human BBS4 peptides (QFPVSTESQKPRQKK and VESSPTETSEQIREK). We affinity-purified the immune serum by passing it through a Sepharose bead column conjugated to the respective peptides (CovalAb, Cambridge). We also used mouse monoclonal antibodies to Myc (ClonTech), HA (ROCHE) and porin (Molecular Probes), antibodies to acetylated tubulin and α-tubulin (both from Sigma), mouse monoclonal or rabbit polyclonal antibody to γ-tubulin (Sigma) and rabbit polyclonal antibody to GFP (Clontech). We used secondary antibodies to rabbit and to mouse conjugated with Alexa Fluor 488 and 594 (Molecular Probes). The rabbit polyclonal antibody to PCM-1 was a gift from A. Merdes (University of Edinburgh).

**Mammalian cell culture and synchronization.** We maintained HeLa, HEK 293, NIH 3T3 and COS-7 cells in Dulbecco's modified Eagle medium (DMEM; Gibco BRL) supplemented with 10% fetal bovine serum (FBS) at 37 °C in 5%

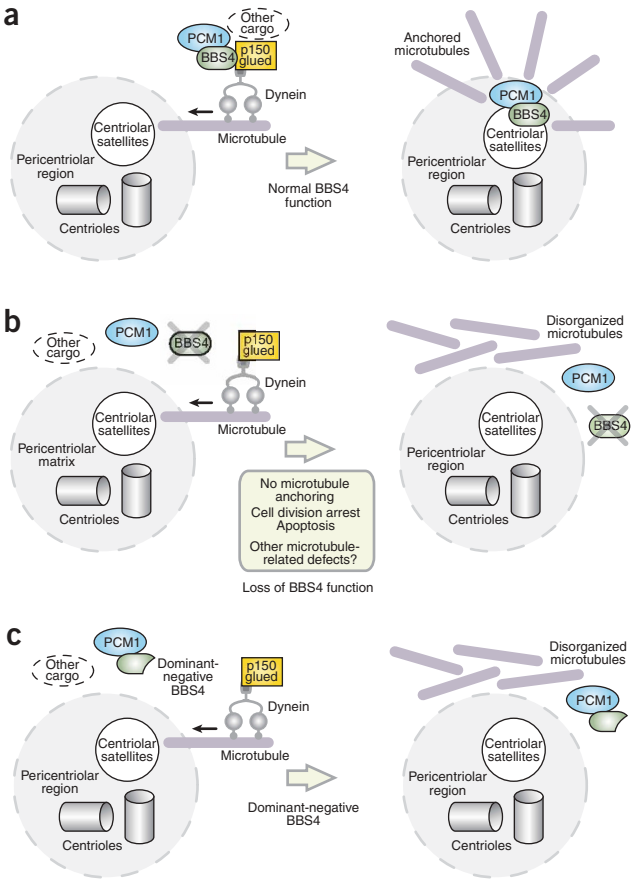


**Figure 8** Model of BBS4 (dys)function. (**a**) Normal BBS4 function. BBS4 recruits PCM1 and associated cargo to the centriolar satellites in a dynein-dependent manner, probably through its interaction with p150$^{glued}$. (**b**) In the absence of BBS4, PCM1 and possibly its cargo do not localize to the centriolar satellites, leading to several cellular phenotypes. (**c**) Some BBS4 truncation mutants have an equally detrimental effect by inhibiting PCM1 localization to the centriolar satellites.

$CO_2$. We maintained mouse kidney collecting duct epithelial cells (IMCD-3) in 1:1 mixture of DMEM and Ham's F12 medium (Gibco BRL) with 10% FBS at 37 °C in 5% $CO_2$. For cell synchronization, we grew HeLa cells in 2 mM thymidine (Sigma) for 18 h, washed them with phosphate-buffered saline (PBS) and grew them in fresh medium without thymidine for 8 h. We then incubated cells with 2 mM thymidine for 18 h, transferred them to fresh medium and fixed them at various time points to monitor cell cycle progression.

**Sucrose density gradient centrifugation.** We collected HEK 293 cells into 10 ml of cold PBS, pelleted them and washed them in PBS and cold TES buffer (20 mM Tris (pH 7.4), 5 mM EDTA, 250 mM Sucrose, 1 protease inhibitor without EDTA (Roche Diagnostics)). We resuspended the final cell pellet in 700 l of TES buffer lacking or containing 1% Triton X-100. Cells were lysed mechanically on ice by passing them through a 27-gauge needle 60 times. Cells in Triton-containing buffer were vortexed and incubated on ice for 30 min. We loaded 300 l of each cell lysate on top of discontinuous sucrose gradients comprising ten steps of 300 l each, prepared in 20 mM Tris (pH 7.4), 10% glycerol and appropriate amount of sucrose. We centrifuged the samples at 100,000*g* for 16 h at 4 °C. We collected fractions (300 l) from the top and subjected them to western-blot analysis.

**Coimmunoprecipitations.** We cloned the open reading frame of BBS4 and a partial cDNA fragment encoding the last 450 amino acids of PCM1 (residues 1,574–2,024) into the pCMV-Myc and pCMV-HA expression vectors (Invitrogen) and confirmed this by sequencing. We transfected HEK 293 cells by calcium phosphate and collected them 48 h after transfection in coimmunoprecipitation buffer (150 mM NaCl, 50 mM TRIS-HCl (pH 7.5) and 1% Nonidet P-40) supplemented with protease inhibitor (Roche) and 1 mM sodium orthovanadate. We incubated cell lysates overnight with 10 g of monoclonal antibody to Myc immobilized on sepharose beads (Covance). We washed immunoprecipitates three times with coimmunoprecipitation buffer, resuspended them in loading buffer and analyzed them by western blotting. We blocked immunoblot PVDF membranes with 0.2% Tween 20 in PBS and 5% milk and probed them with appropriate antibodies. We used ECL (Amersham) for detection.

**Fluorescence microscopy.** We grew cells on glass coverslips, rinsed them in PBS, fixed them in methanol at –20 °C for 10 min and blocked them in PBS with 5.5% FBS for 60 min at room temperature. We then incubated cells for 60 min at room temperature with the relevant primary antibody diluted in PBS. Antibody binding was visualized with secondary antibodies conjugated to Alexa Fluor 488 or 594. We counterstained nuclei with DAPI. We mounted slides in Prolong antifade reagent (Molecular Probes) and observed them by fluorescence microscopy using standard epifluorescence, Leica TCS SP confocal or Olympus Deltavision microscope systems.

**Transmission electron microscopy.** After primary labeling of cells with affinity-purified BBS4 antibody, we labeled HEK 293 cells with secondary goat antibody to rabbit IgG conjugated to 1-nm-particle gold (BBInternational). We silver-enhanced the cells (Silver Enhancing Kit, BBInternational), fixed them in 3% glutaraldehyde (EM grade, Agar Scientific) in 0.1 M sodium cacodylate and 5 mM $CaCl_2$, post-fixed them with 1% aqueous $OsO_4$ and dehydrated them with ascending grades of ethanol. We then impregnated cells with Araldite resin mixture:ethanol in 50:50 ratio (20 ml of Araldite CY212, 25 ml of DDSA and 0.8 ml of DMP30; Agar Scientific). We polymerized the preparation at 60 °C for 2 d. We cut the resultant thin resin-cell films, mounted them onto resin blanks before ultrathin sectioning using a diamond knife on a Reichert Ultracut microtome and collected the sections on 400 mesh copper grids. We stained them with 25% uranyl acetate in methanol (Analar) followed by Reynolds Lead Citrate. We viewed sections with a JEOL 120 EX transmission electron microscope.

**Knockdown of *BBS4* expression by RNAi: oligonucleotide-based method.** We designed DNA oligonucleotides (21-mers) specific to BBS4 with an online tool. These corresponded to human *BBS4* nucleotides 27–48 (Si27), 566–587 (Si566), 831–852 (Si831) and 2,025–2,046 (Si2025). We used each oligonucleotide to synthesize specific siRNAs according to the manufacturer's instructions (*Silencer* siRNA Construction Kit, Ambion). Before transfection, we grew HeLa cells overnight in DMEM with 10% FBS (antibiotic-free) on chamber glass slides and transfected them with Lipofectamine2000 (Invitrogen) in 250 l of a OPTIMEM and DMEM mix (1:5; Life Technologies). The final concentration was 1 nM siRNA in cells plated at a density of 1 $10^4$ over a glass substrate area of 1.8 $cm^2$. After 4 h, we expanded the medium with DMEM and FBS (10% final concentration). We incubated the chambers for 48 h before fixing and processing the cells for immunofluorescence analysis.

**Knockdown of *BBS4* expression by RNAi: pSUPER vector method.** We cloned sense and antisense primers corresponding to human *BBS4* into a mammalian expression vector (pSUPER) as described[29]. We seeded HeLa cells on six-well plates and cotransfected them with 0.1 g of a neomycin-containing plasmid (pcDNA3.1, Invitrogen) and 1 g of either pSUPER-BBS4 or pSUPER empty vector. We split the HeLa cells onto coverslips at a 1:5 ratio into growth medium with 500 g of G418 activity per ml (Gibco) 24 h after transfection. We maintained transfected cells in culture for 4–5 d in G418 before collecting them.

**Knockdown of *BBS4* expression by RNAi: pSilencer vector method.** We used pSilencer 2.1-U6 neo siRNA expression vector (Ambion) to generate siRNA against BBS4 by ligating annealed oligonucleotides into *Hin*dIII and *Bam*HI sites. We introduced the resulting construct into COS-7 cells and subjected them to neomycin selection (500 g activity per ml) for 9 d. Primer sequences are available on request.

**Microtubule regrowth assays.** We treated HeLa cells transfected with pSUPER-BBS4 or pSUPER empty vector with 25 M nocodazole at 37 °C for 1 h. After removing the drug, we incubated the cells for various times to allow microtubules to regrow, as visualized by immunofluorescence microscopy using an antibody to α-tubulin.

**FACS analyses.** We transfected COS-7 cells with pSilencer-BBS4 constructs and cultured them in DMEM with 500 g ml$^{-1}$ G418 for 9 d, removed them from plates by trypsin digestion and fixed them in 75% ethanol. We stained fixed cells in PBS containing 3.8 mM sodium citrate, 50 g ml$^{-1}$ propidium iodide and 500 ng ml$^{-1}$ RNase A. We analyzed samples with the FACSCalibur system (Becton Dickinson).

**TUNEL assay.** HeLa cells were untreated or treated with BBS4 siRNA or a control scrambled siRNA. We fixed cells in 4% paraformaldehyde (30 min), blocked them with 3% $H_2O_2$ in methanol (10 min) and permeabilized them with 0.1% Triton X-100. We then identified DNA strand breaks by labeling free 3′-OH termini with a fluorescein-conjugated nucleotide (dUTP) using terminal deoxynucleotidyl transferase (In Situ Cell Death Detection Kit, Roche). We scored apoptosis by counting the number of typical apoptotic cells per high-power field (60 ) under fluorescence microscopy. We calculated the mean number of cells in 10 fields per cell preparation.

**Immunohistochemistry.** We incubated consecutive 5- m-thick sections of adult (postnatal day 12–18) mouse organs or mouse embryos (embryonic day (E) 12.5–16.5) with polyclonal antibodies against BBS4 and PCM1 diluted to 1:750 and 1:1,000, respectively. Hybridization, washes and staining procedures were as described[18].

**URL.** The oligonucleotide design tool that we used is available at http://www.ambion.com/techlib/misc/silencer_siRNA_template.html.

*Note: Supplementary information is available on the Nature Genetics website.*

ACKNOWLEDGMENTS

We thank C. Beh and S. Huston for their critical evaluation of this manuscript and P. Scambler for discussions. This study was supported in part by a National Institute of Child Health and Development, National Institutes of Health grant and the March of Dimes (N.K.); National Cancer Institute of Canada (Terry Fox Run) and Heart and Stroke Foundation of BC and Yukon (M.R.L.); the National Kidney Research Fund (B.E.H.); and the Birth Defects Foundation and the Wellcome Trust (P.L.B.). P.L.B. is a Wellcome Trust Senior Research Fellow. J.C.K. and M.A.E. hold scholarships from the Michael Smith Foundation for Health Research and Heart and Stroke Foundation of Canada, respectively, and M.R.L. is the recipient of scholar awards from the Canadian Institutes of Health Research and Michael Smith Foundation for Health Research.

COMPETING INTERESTS STATEMENT

The authors declare that they have no competing financial interests.

Received 16 January; accepted 24 March 2004
Published online at http://www.nature.com/naturegenetics/

1. Zimmerman, W., Sparks, C.A. & Doxsey, S.J. Amorphous no longer: the centrosome comes into focus. *Curr. Opin. Cell Biol.* **11**, 122–128 (1999).
2. Zimmerman, W. & Doxsey, S.J. Construction of centrosomes and spindle poles by molecular motor-driven assembly of protein particles. *Traffic* **1**, 927–934 (2000).
3. Ou, Y.Y., Zhang, M., Chi, S., Matyas, J.R. & Rattner, J.B. Higher order structure of the PCM adjacent to the centriole. *Cell Motil. Cytoskeleton* **55**, 125–133 (2003).
4. Kubo, A., Sasaki, H., Yuba-Kubo, A., Tsukita, S. & Shiina, N. Centriolar satellites: Molecular characterization, ATP-dependent movement toward centrioles and possible involvement in ciliogenesis. *J. Cell Biol.* **147**, 969–979 (1999).
5. Rattner, J.B. Ultrastructure of centrosome domains and identification of their protein components. in *In The Centrosome* (ed. Kalnins, V.I.) 45–69 (Academic, San Diego, 1992).
6. Bobinnec, Y. *et al.* Centriole disassembly in vivo and its effect on centrosome structure and function in vertebrate cells. *J. Cell Biol.* **143**, 1575–1589 (1998).
7. Beisson, J. & Wright, M. Basal body/centriole assembly and continuity. *Curr. Opin. Cell Biol.* **15**, 96–104 (2003).
8. Balczon, R., Bao, L. & Zimmer, W.E. PCM-1, A 228-kD centrosome autoantigen with a distinct cell cycle distribution. *J. Cell Biol.* **124**, 783–793 (1994).
9. Dammermann, A. & Merdes, A. Assembly of centrosomal proteins and microtubule organization depends on PCM-1. *J. Cell Biol.* **159**, 255–266 (2002).
10. Beales, P.L., Elcioglu, N., Woolf, A.S., Parker, D. & Flinter, F.A. New criteria for improved diagnosis of Bardet-Biedl syndrome: results of a population survey. *J. Med. Genet.* **36**, 437–446 (1999).
11. Katsanis, N. *et al.* Triallelic inheritance in Bardet-Biedl syndrome, a mendelian recessive disorder. *Science* **293**, 2256–2259 (2001).
12. Badano, J.L. *et al.* Identification of a novel Bardet-Biedl syndrome protein, BBS7, that shares structural features with BBS1 and BBS2. *Am. J. Hum. Genet.* **72**, 650–658 (2003).
13. Mykytyn, K. *et al.* Identification of the gene (*BBS1*) most commonly involved in Bardet-Biedl syndrome, a complex human obesity syndrome. *Nat. Genet.* **31**, 435–438 (2002).
14. Mykytyn, K. *et al.* Identification of the gene that, when mutated, causes the human obesity syndrome BBS4. *Nat. Genet.* **28**, 188–191 (2001).
15. Nishimura, D.Y. *et al.* Positional cloning of a novel gene on chromosome 16q causing Bardet-Biedl syndrome (BBS2). *Hum. Mol. Genet.* **10**, 865–874 (2001).
16. Katsanis, N. *et al.* Mutations in MKKS cause obesity, retinal dystrophy and renal malformations associated with Bardet-Biedl syndrome. *Nat. Genet.* **26**, 67–70 (2000).
17. Slavotinek, A.M. *et al.* Mutations in MKKS cause Bardet-Biedl syndrome. *Nat. Genet.* **26**, 15–16 (2000).
18. Ansley, S.J. *et al.* Basal body dysfunction is a likely cause of pleiotropic Bardet-Biedl syndrome. *Nature* **425**, 628–633 (2003).
19. Rosenbaum, J.L. & Witman, G.B. Intraflagellar transport. *Nat. Rev. Mol. Cell Biol.* **3**, 813–825 (2002).
20. Schultz, J., Copley, R.R., Doerks, T., Ponting, C.P. & Bork, P. SMART: a web-based tool for the study of genetically mobile domains. *Nucleic Acids Res.* **28**, 231–234 (2000).
21. Blatch, G.L. & Lassle, M. The tetratricopeptide repeat: a structural motif mediating protein-protein interactions. *Bioessays* **21**, 932–939 (1999).
22. Moudjou, M., Bordes, N., Paintrand, M. & Bornens, M. gamma-Tubulin in mammalian cells: the centrosomal and the cytosolic forms. *J. Cell Sci.* **109**, 875–887 (1996).
23. Dictenberg, J.B. *et al.* Pericentrin and gamma-tubulin form a protein complex and are organized into a novel lattice at the centrosome. *J. Cell Biol.* **141**, 163–174 (1998).
24. Vaughan, K.T. & Vallee, R.B. Cytoplasmic dynein binds dynactin through a direct interaction between the intermediate chains and p150$^{Glued}$. *J. Cell Biol.* **131**, 1507–1516 (1995).
25. Valle, R.D. The molecular motor toolbox for intracellular transport. *Cell* **112**, 467–480 (2003).
26. Waterman-Storer, C.M., Karki, S. & Holzhbaur, E.L. The p150$^{Glued}$ component of the dynactin complex binds to both microtubules and the actin-related protein centractin (Arp-1). *Proc. Natl. Acad. Sci. USA* **92**, 1634–1638 (1995).
27. Balczon, R., Varden, C.E. & Schroer, T.A. Role for microtubules in centrosome doubling in Chinese hamster ovary cells. *Cell Motil. Cytoskeleton* **42**, 60–72 (1999).
28. Young, A., Dictenberg, J.B., Purohit, A., Tuft, R. & Doxsey, S.J. Cytoplasmic dynein-mediated assembly of pericentrin and gamma tubulin onto centrosomes. *Mol. Biol. Cell* **11**, 2047–2056 (2000).
29. Brummelkamp, T.R., Bernards, R., Agami, R. A system for stable expression of short interfering RNAs in mammalian cells. *Science* **296**, 550–553 (2002).